Simplified Cluster Voltage Balancing Control Based on Zero-sequence Voltage Injection for Star-connected Cascaded H-bridge STATCOM

Kai Hu, Guoliang Zhao, *Member*, *CSEE*, Daorong Lu, Zhengang Lu, *Senior Member*, *CSEE*, Nianwen Xiang, *Member*, *IEEE*, Shulai Wang, and Jintian Lin

***Abstract*—The cluster DC voltage balancing control adopting zero-sequence voltage injection is appropriate for the star-connected cascaded H-bridge STATCOM because no zero-sequence currents are generated in the three-phase three-wire system. However, as the zero-sequence voltage is expressed in trigonometric form, traditional control methods involve many complicated operations, such as the square-root, trigonometric operations, and inverse tangent operations. To simplify cluster voltage balancing control, this paper converts the zero-sequence voltage to the dq frame in a DC representation by introducing a virtually orthogonal variable, and the DC components of the zero-sequence voltage in the dq frame are regulated linearly by proportional integral regulators, rather than being calculated from uneven active powers in traditional controls. This removes all complicated operations. Finally, this paper presents simulation and experimental results for a 400 V/±7.5 kvar star-connected STATCOM, in balanced and unbalanced scenarios, thereby verifying the effectiveness of the proposed control.**

***Index Terms*—Cluster DC voltage balancing control, DC representation of zero-sequence voltage, star-connected cascaded H-bridge STATCOM, zero-sequence voltage injection.**

I. Introduction

THE Cascaded H-Bridge (CHB) converter is widely used for static synchronous compensator (STATCOM) in a power system owing to its modularity and good harmonic performance [1]–[3]. It has two typical structures, namely the star connection and delta connection. These structures have different merits in terms of voltage and current rating, number of cells, and negative-sequence current [4], [5]. In compensating negative-sequence current to the grid, the star connection has a smaller negative-sequence current compensation range than a delta connection [6], [7]. Hence, the star-connected CHB STATCOM is considered suitable for positive-sequence reactive power compensation to regulate grid voltages.

However, imbalance of DC voltages among the three clusters is a great challenge for the star-connected CHB STATCOM. This imbalance is caused by nonuniformity of all cells and the unbalanced power grid [8]–[10]. Many interesting control methods have been presented in past years to achieve cluster voltage balance. These can be divided into two categories: one is the negative-sequence (voltage or current) injection [11]–[15], and the other is the zero-sequence voltage injection [7], [16]–[22]. Both methods redistribute active power among the three clusters by generating unbalanced active powers to achieve cluster DC voltage balance. However, the main disadvantage of the negative-sequence (voltage or current) injection is that negative-sequence current injected into the grid affects power quality adversely. In contrast, zero-sequence voltage injection does not lead to unbalanced currents owing to three-phase and three-wire configuration. Hence, from this viewpoint, zero-sequence voltage injection is more attractive than negative-sequence injection.

In a traditional strategy, zero-sequence voltage is obtained by establishing the relationship between the inhomogeneous active powers and zero-sequence voltage, by applying proportional integral (PI) regulators to errors between the actual feedback cluster voltage and its reference cluster voltage; the inhomogeneous active powers of three clusters can be obtained. On this basis, zero-sequence voltage can be derived explicitly. However, in Refs. [7], [16], [17], this calculation incorporates many divisions and inverse tangent operations owing to the trigonometric expression of all variables in the abc frame. This significantly increases calculation burden on a controller based on a digital signal processor (DSP) or field-programmable gate array (FPGA). To simplify calculation, researchers adopted a stationary $\alpha\beta$ frame, and thus derived an orthogonal component aligned to the zero-sequence voltage [18]–[20]. Using these two orthogonal components greatly reduced division operation counts. Unfortunately, a square root operation was introduced, which also consumes a lot of controller resources. Chen *et al*. [21] used the $dq0$ frame, which still does not get rid of the complicated operations. In [22], an interesting approach was proposed whereby the zero-sequence voltage

Manuscript received April 18, 2022; revised July 2, 2022; accept August 3, 2022. Date of online publication October 12, 2022; date of current version September 11, 2024. This work is supported by National Key R&D Program of China (No. 2021YFB2401100) and the Science and Technology Project of State Grid Corporation of China (No. 5211DS22002C).

K. Hu (ORCID: https://orcid.org/0000-0001-9044-8172), N. W. Xiang and S. L. Wang are with School of Electrical Engineering and Automation, Hefei University of Technology, Hefei 230009, China.

D. R. Lu (corresponding author, email: tcludaorong@nuaa.edu.cn) is with the School of Electrical and Automation Engineering, Nanjing Normal University, Nanjing 210023, China.

G. L. Zhao and Z. G. Lu are with State Grid Smart Grid Research Institute (SGRI), Beijing 102209, China.

J. T. Lin is with the Power grid Technology Center of State Grid Zhejiang Electric Power Research Institute, Hangzhou 310004, China.

DOI: 10.17775/CSEEJPES.2022.01700

is converted into the dq frame to achieve DC representation. This eliminates the inverse tangent and square root operations, which greatly reduces calculation burden. However, division operation is still involved. In summary, traditional methods achieve cluster DC voltage balance by increasing complexity of the control, which results in introducing complex operations (e.g., square root, trigonometric operations, and inverse trigonometric operations) into the control strategy. There are two reasons for the existence of complex operations: first is that zero-sequence voltage in traditional methods is expressed in a trigonometric form, which will thus necessitate inclusion of inverse trigonometric operations and square root operations in the calculation, and second is that zero-sequence voltage is calculated indirectly by a traditional method based on active powers, which introduce additional complexity to the algorithm. These complex operations demand more controller resources than ordinary operations (addition, subtraction, and multiplication) and therefore increase calculation burden on the DSP- or FPGA-based controllers.

This paper proposes a linear and simplified cluster voltage balancing control based on zero-sequence voltage injection that simplifies the control strategy and eliminates all the complex operations mentioned above, while also maintaining cluster DC voltage balance. Our control method eliminates complex operations in two ways. First, zero-sequence voltage is expressed within a rotated dq frame, which removes the complex operations. Second, we establish a linear relationship between cluster DC voltage errors and active powers, which means the d-axis and q-axis components of the zero-sequence voltage are regulated linearly by PI regulators, and feedback control and feedforward control strategies generate zero-sequence modulated voltages directly, rather than generate the active powers required for complex operations. To achieve a regulation mechanism, we establish a generalized and coupled relationship between the DC components of the zero-sequence voltage and the cluster DC voltage error by introducing four proportional regulators. In this relationship, ranges of the proportional parameters are derived according to the principle of cluster voltage balance. To simplify design of the proportional parameters and reduce control coupling, we propose a simple and linear cluster voltage balancing control with only one PI regulator. The proposed method is much simpler than traditional methods, therefore the proposed method can be implemented in low-level DSP and FPGA-based controllers and helps engineers develop a control system easily and quickly in practice. Finally, validity of the proposed balancing control is verified by MATLAB/Simulink simulation and experiments on a 400 V/7.5 kVar star-connected CHB STATCOM prototype.

II. Cluster DC Voltage Balancing Control Strategy

A. System Overview

The circuit configuration of a general star-connected CHB STATCOM with N cascaded H-bridge cells per cluster is shown in Fig. 1. A typical hierarchical control structure for the CHB STATCOM is used. This structure has three layers, as shown in Fig. 2. The first layer, dq dual-loop decoupling current control [22], not only controls reactive currents but also regulates active power exchange between STATCOM and the grid by controlling the d-axis current components to stabilize overall DC voltage. The second layer, cluster DC voltage balancing control, is dedicated to balancing the three cluster voltages (U_{dca}, U_{dcb}, and U_{dcc}) by injecting the zero-sequence voltage. Finally, the third layer, individual voltage balancing control, is devoted to regulating the voltage of each cell ($U_{\mathrm{dck}j}$) by superimposing an active voltage vector [23].

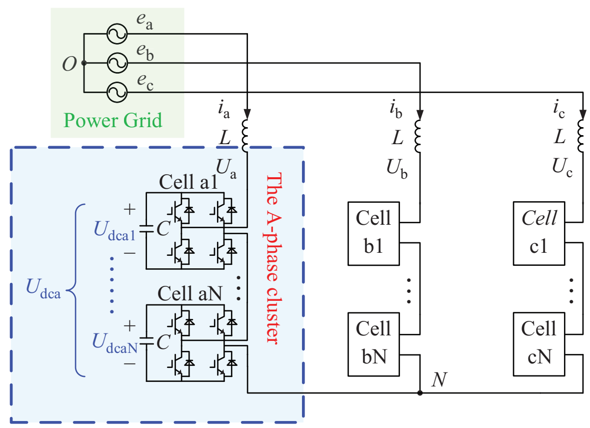

Fig. 1. Circuit configuration of the star-connected CHB STATCOM.

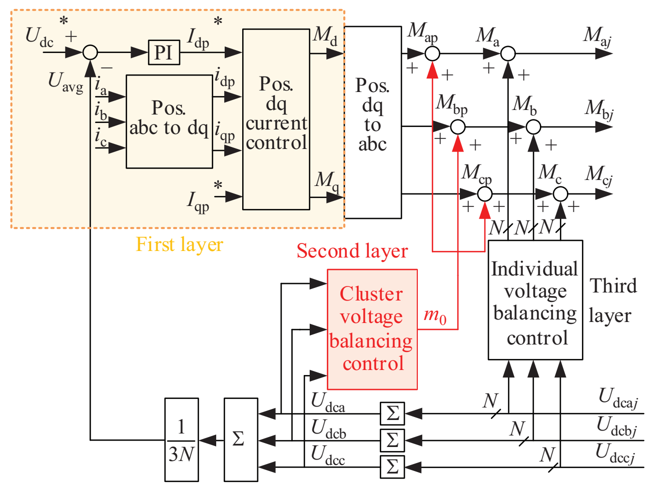

Fig. 2. The control structure of the star-connected CHB STATCOM.

B. Active Powers Distribution Under Unbalanced Grid Voltages

The unbalanced grid voltages can be written as:

$$\begin{aligned}\begin{bmatrix} e_{\mathrm{a}} \\ e_{\mathrm{b}} \\ e_{c} \end{bmatrix} &= \begin{bmatrix} e_{\mathrm{ap}} \\ e_{\mathrm{bp}} \\ e_{c p} \end{bmatrix} + \begin{bmatrix} e_{\mathrm{an}} \\ e_{\mathrm{bn}} \\ e_{\mathrm{cn}} \end{bmatrix} \\ &= \begin{bmatrix} \cos(\omega t) & -\sin(\omega t) \\ \cos\left(\omega t - \frac{2}{3}\pi\right) & -\sin\left(\omega t - \frac{2}{3}\pi\right) \\ \cos\left(\omega t + \frac{2}{3}\pi\right) & -\sin\left(\omega t + \frac{2}{3}\pi\right) \end{bmatrix} \begin{bmatrix} E_{\mathrm{dp}} \\ E_{\mathrm{qp}} \end{bmatrix}\end{aligned}$$

$$+\begin{bmatrix}\cos(\omega t) & \sin(\omega t)\\ \cos\left(\omega t+\frac{2}{3}\pi\right) & \sin\left(\omega t+\frac{2}{3}\pi\right)\\ \cos\left(\omega t-\frac{2}{3}\pi\right) & \sin\left(\omega t-\frac{2}{3}\pi\right)\end{bmatrix}\begin{bmatrix}E_{\mathrm{dn}}\\ E_{\mathrm{qn}}\end{bmatrix} \quad (1)$$

Here, subscripts d and q stand for the components along with the d- and q-axes, respectively; subscripts p and n denote the positive- and negative-sequence components, respectively; and ω is the fundamental angular frequency of the grid voltage. It is noted that zero-sequence grid voltage does not affect STATCOM operation owing to the three-phase and three-wire structure.

In the presence of unbalanced grid voltage, the converter should generate positive-, negative- and zero-sequence voltages synchronously to suppress negative-sequence currents. High-switching-frequency components of the converter output voltage are ignored so that converter output voltages are represented in the dq frame as:

$$\begin{bmatrix}u_{\mathrm{a}}\\ u_{\mathrm{b}}\\ u_{c}\end{bmatrix}=\begin{bmatrix}\cos(\omega t) & -\sin(\omega t)\\ \cos(\omega t-\frac{2}{3}\pi) & -\sin(\omega t-\frac{2}{3}\pi)\\ \cos(\omega t+\frac{2}{3}\pi) & -\sin(\omega t+\frac{2}{3}\pi)\end{bmatrix}\cdot\begin{bmatrix}U_{\mathrm{dp}}\\ U_{\mathrm{qp}}\end{bmatrix}$$
$$+\begin{bmatrix}\cos(\omega t) & \sin(\omega t)\\ \cos(\omega t+\frac{2}{3}\pi) & \sin(\omega t+\frac{2}{3}\pi)\\ \cos(\omega t-\frac{2}{3}\pi) & \sin(\omega t-\frac{2}{3}\pi)\end{bmatrix}\cdot\begin{bmatrix}U_{\mathrm{dn}}\\ U_{\mathrm{qn}}\end{bmatrix}+\begin{bmatrix}u_0\\ u_0\\ u_0\end{bmatrix} \quad (2)$$

Subscript 0 denotes the zero-sequence components. To express zero-sequence voltage in the dq frame as a DC form rather than as a magnitude and phase angle, similar to the case for the positive- and negative-sequence voltages, we introduce a virtual quadrature zero-sequence voltage with a 90° delay with respect to the original zero-sequence voltage [22]. Subsequently, the zero-sequence voltage is transformed to the dq frame via the PARK transformation as:

$$\begin{bmatrix}u_0\\ u_{0\_\mathrm{delay}}\end{bmatrix}=\begin{bmatrix}\cos(\omega t) & -\sin(\omega t)\\ \sin(\omega t) & \cos(\omega t)\end{bmatrix}\cdot\begin{bmatrix}U_{\mathrm{d0}}\\ U_{\mathrm{q0}}\end{bmatrix} \quad (3)$$

This paper mainly focuses on the balanced output currents without negative-sequence components. To balance the three-phase currents, we force the converter output negative-sequence voltages to be equal to the negative-sequence voltages of the grid ($E_{\mathrm{dn}}=U_{\mathrm{dn}}$, $E_{\mathrm{qn}}=U_{\mathrm{qn}}$) and thus limiting the negative-sequence currents to zero. In this scenario, the converter output negative-sequence voltages and positive-sequence currents generate uneven active powers, further affecting distribution of active powers among the three clusters. This is derived as:

$$\begin{bmatrix}P_{\mathrm{an}}\\ P_{\mathrm{bn}}\\ P_{\mathrm{cn}}\end{bmatrix}=\begin{bmatrix}\frac{\omega}{2\pi}\int_0^{\frac{2\pi}{\omega}}(u_{\mathrm{an}}\cdot i_{\mathrm{ap}})\mathrm{d}t\\ \frac{\omega}{2\pi}\int_0^{\frac{2\pi}{\omega}}(u_{\mathrm{bn}}\cdot i_{\mathrm{bp}})\mathrm{d}t\\ \frac{\omega}{2\pi}\int_0^{\frac{2\pi}{\omega}}(u_{\mathrm{cn}}\cdot i_{\mathrm{cp}})\mathrm{d}t\end{bmatrix}$$
$$=\begin{bmatrix}\frac{I_{\mathrm{dp}}}{2} & -\frac{I_{\mathrm{qp}}}{2}\\ \frac{-I_{\mathrm{dp}}-\sqrt{3}I_{\mathrm{qp}}}{4} & \frac{I_{\mathrm{qp}}-\sqrt{3}I_{\mathrm{dp}}}{4}\\ \frac{-I_{\mathrm{dp}}+\sqrt{3}I_{\mathrm{qp}}}{4} & \frac{I_{\mathrm{qp}}+\sqrt{3}I_{\mathrm{dp}}}{4}\end{bmatrix}\cdot\begin{bmatrix}E_{\mathrm{dn}}\\ E_{\mathrm{qn}}\end{bmatrix} \quad (4)$$

Here, i_{ap}, i_{bp} and i_{cp} are the positive-sequence currents in the abc frame and I_{dp} and I_{qp} are the positive-sequence currents in the dq frame. CHB STATCOM mainly exchanges reactive power with the grid, the rated reactive power is much larger than the active power absorbed from the grid owing to losses, and it is reasonable to approximate I_{dp} as zero. Hence, the active powers in (4) can be simplified as:

$$\begin{bmatrix}P_{\mathrm{an}}\\ P_{\mathrm{bn}}\\ P_{\mathrm{cn}}\end{bmatrix}=\begin{bmatrix}0 & -\frac{I_{\mathrm{qp}}}{2}\\ \frac{-\sqrt{3}I_{\mathrm{qp}}}{4} & \frac{I_{\mathrm{qp}}}{4}\\ \frac{\sqrt{3}I_{\mathrm{qp}}}{4} & \frac{I_{\mathrm{qp}}}{4}\end{bmatrix}\cdot\begin{bmatrix}E_{\mathrm{dn}}\\ E_{\mathrm{qn}}\end{bmatrix} \quad (5)$$

Equation (5) shows the three-phase active powers generated by negative-sequence voltages and that generated by positive-sequence currents are not equal. However, their sum is zero. This shows they do not affect the total active power exchange, i.e., they do not affect overall DC voltage but cause an unbalanced cluster DC voltage.

Injection of the zero-sequence voltage redistributes active powers in the three clusters and further balances the DC voltage of the three clusters. Therefore, considering (3), the three-phase active powers generated by the zero-sequence voltages and the positive-sequence currents are derived as:

$$\begin{bmatrix}P_{\mathrm{a0}}\\ P_{\mathrm{b0}}\\ P_{\mathrm{c0}}\end{bmatrix}=\begin{bmatrix}\frac{\omega}{2\pi}\int_0^{\frac{2\pi}{\omega}}u_0\cdot i_{\mathrm{ap}}\mathrm{d}t\\ \frac{\omega}{2\pi}\int_0^{\frac{2\pi}{\omega}}u_0\cdot i_{\mathrm{bp}}\mathrm{d}t\\ \frac{\omega}{2\pi}\int_0^{\frac{2\pi}{\omega}}u_0\cdot i_{\mathrm{cp}}\mathrm{d}t\end{bmatrix}=\begin{bmatrix}0 & \frac{I_{\mathrm{qp}}}{2}\\ \frac{\sqrt{3}I_{\mathrm{qp}}}{4} & \frac{-I_{\mathrm{qp}}}{4}\\ \frac{-\sqrt{3}I_{\mathrm{qp}}}{4} & \frac{-I_{\mathrm{qp}}}{4}\end{bmatrix}\cdot\begin{bmatrix}U_{\mathrm{d0}}\\ U_{\mathrm{q0}}\end{bmatrix} \quad (6)$$

We can see that (6) is similar to (5) in that the three-phase active powers generated by the zero-sequence voltages (U_{d0}, U_{q0}) are also unequal. However, the sum power is zero, which means the zero-sequence voltage injection redistributes the active power of the three-phase clusters linearly and without affecting the overall active power exchange, realizing decoupling from the first layer of control, such that DC voltages of the three clusters can be balanced. Furthermore, because currents in the active power calculations are positive-sequence currents and the negative-sequence currents do not exist in this case, the uneven active powers generated by the negative-sequence currents are not considered. Therefore, the proposed method is more suitable for application to positive-sequence current injection rather than negative-sequence current injection.

C. Linear Regulation Mechanism for Cluster DC Voltage Balancing Control based on Zero-sequence Voltage Injection

The relationship between zero-sequence voltages and active powers has been established linearly in the dq frame, and it is thus essential to establish the relationship between the zero-sequence voltage and the cluster DC voltage. To explore the generalized relationship, we introduce the simplest proportional regulator based on the cluster voltage errors to regulate zero-sequence voltages along the d- and q-axes, as illustrated in Fig. 3 and expressed in (7). It is noted that because the sum of the three-phase cluster voltages is controlled in the first layer, only the cluster voltages in phases A and B are controlled in this layer. This achieves control decoupling between the two layers:

$$\begin{aligned}U_{\mathrm{d0}}&=k_{\mathrm{p1}}\cdot(U_{\mathrm{dca}}-U_{\mathrm{dcref}})+k_{\mathrm{p2}}\cdot(U_{\mathrm{dcb}}-U_{\mathrm{dcref}})\\ U_{\mathrm{q0}}&=k_{\mathrm{p3}}\cdot(U_{\mathrm{dca}}-U_{\mathrm{dcref}})+k_{\mathrm{p4}}\cdot(U_{\mathrm{dcb}}-U_{\mathrm{dcref}})\end{aligned} \quad (7)$$

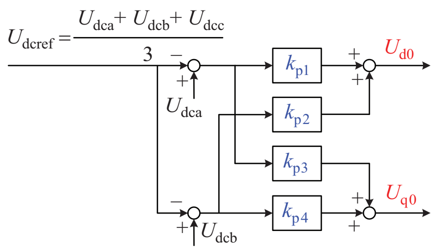

Fig. 3. Generalized linear correlation between the zero-sequence voltage and the cluster DC voltages.

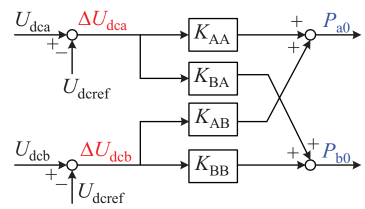

Fig. 4. Relationship between the cluster active powers and the cluster voltage errors.

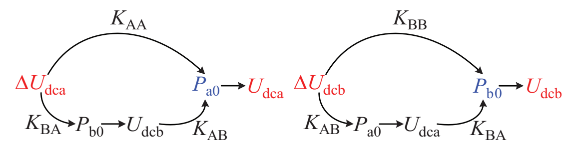

Fig. 5. Two closed loops of regulating the cluster voltages.

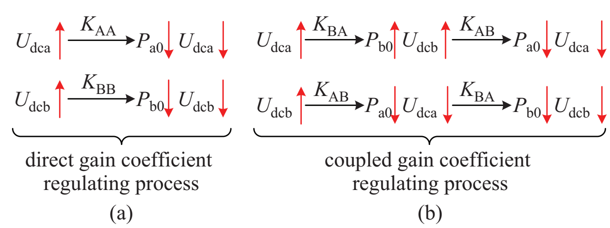

Fig. 6. Closed-loop regulating mechanism of the clustered voltages.

By substituting (7) into (6), active powers generated by the zero-sequence voltage in phases A and B are rewritten as:

$$
\begin{aligned}
P_{\mathrm{a0}} &= \left[\frac{1}{2}k_{\mathrm{p3}}(U_{\mathrm{dca}}-U_{\mathrm{dcref}})+\frac{1}{2}k_{\mathrm{p4}}(U_{\mathrm{dcb}}-U_{\mathrm{dcref}})\right]\cdot I_{\mathrm{qp}}\\
P_{\mathrm{b0}} &= \left[\left(\frac{\sqrt{3}}{4}k_{\mathrm{p1}}-\frac{1}{4}k_{\mathrm{p3}}\right)(U_{\mathrm{dca}}-U_{\mathrm{dcref}})\right.\\
&\quad \left.+\left(\frac{\sqrt{3}}{4}k_{\mathrm{p2}}-\frac{1}{4}k_{\mathrm{p4}}\right)(U_{\mathrm{dcb}}-U_{\mathrm{dcref}})\right]\cdot I_{\mathrm{qp}}
\end{aligned}
\tag{8}
$$

Equation (8) shows the correlation between the active powers and the cluster voltage errors, which illustrates that active power is determined by proportional parameters and reactive current. For the reactive power current, I_{qp} can be either positive or negative, which is determined by the operation mode of STATCOM. To determine the range of proportional parameters, I_{qp} is first assumed to be positive. Equation (8) is illustrated in Fig. 4 for the sake of analysis, where

$$
\begin{aligned}
K_{\mathrm{AA}} &= \frac{1}{2}k_{\mathrm{p3}}\cdot I_{\mathrm{qp}},\ K_{\mathrm{BB}}=\left(\frac{\sqrt{3}}{4}k_{\mathrm{p2}}-\frac{1}{4}k_{\mathrm{p4}}\right)\cdot I_{\mathrm{qp}}\\
K_{\mathrm{AB}} &= \frac{1}{2}k_{\mathrm{p4}}\cdot I_{\mathrm{qp}},\ K_{\mathrm{BA}}=\left(\frac{\sqrt{3}}{4}k_{\mathrm{p1}}-\frac{1}{4}k_{\mathrm{p3}}\right)\cdot I_{\mathrm{qp}}
\end{aligned}
\tag{9}
$$

In Fig. 4, each cluster voltage error reaches cluster active power through two branches and each branch has a gain coefficient that can be classified as a direct gain coefficient ($K_{\mathrm{AA}}, K_{\mathrm{BB}}$) or coupled gain coefficient ($K_{\mathrm{AB}}, K_{\mathrm{BA}}$). Hence, each cluster voltage regulation has two closed loops, which are illustrated in Fig. 5. One is closely related to the direct gain coefficients and the other is determined by the coupled gain coefficients.

To determine the range of gain coefficients and thus reduce cluster voltage errors, the cluster active power of phase A or B should vary inversely with the cluster voltage in the corresponding phase. Accordingly, it is straightforward to conclude that direct gain coefficients should be negative ($K_{\mathrm{AA}} < 0$, $K_{\mathrm{BB}} < 0$). We take the phase-A cluster voltage as an example for analysis. If the cluster voltage U_{dca} is higher than its reference, multiplying K_{AA} (< 0) by its positive error will yield negative P_{a0}, which reduces the cluster voltage U_{dca}, as illustrated in Fig. 6(a). The same is true for the phase-B cluster voltage U_{dcb}. Hence, negative K_{AA} and K_{BB} can limit deviation of cluster voltages. For the coupled gain coefficients, the signs of K_{AB} and K_{BA} must be opposite according to the regulating loop associated with K_{AB} and K_{BA} in Fig. 5. $K_{\mathrm{AB}} < 0$ and $K_{\mathrm{BA}} > 0$ are taken as an example to analyze phase-A cluster voltage, and the same analysis can be performed under the conditions that $K_{\mathrm{AB}} > 0$ and $K_{\mathrm{BA}} < 0$. Likewise, if cluster voltage U_{dca} is above its reference, its positive error going through the K_{BA} (> 0) branch leads to positive P_{b0}, increasing the phase-B cluster voltage U_{dcb}. This reduces P_{a0} via the K_{AB} (< 0) branch, as illustrated in Fig. 6(b).

Therefore, the induced cluster active power reduces the cluster voltage errors when proportional parameters ($k_{\mathrm{p1}}, k_{\mathrm{p2}}, k_{\mathrm{p3}}, k_{\mathrm{p4}}$) are properly designed such that direct and coupled gain coefficients meet inequalities (10) and (11). DC voltages of three clusters can be equalized as long as the cluster active power is sufficiently high:

$$K_{\mathrm{AA}} < 0,\ K_{\mathrm{BB}} < 0 \tag{10}$$

$$K_{\mathrm{AB}}\cdot K_{\mathrm{BA}} < 0 \tag{11}$$

However, the aforementioned analysis is based on a positive reactive power current I_{qp}. When reactive power current is negative, we need to redesign these four parameters to satisfy inequalities (10) and (11). In addition, four regulators need to be designed, which complicates the proposed strategy.

D. Simple Cluster DC Voltage Balancing Control Method

To solve the above two problems and make the design easier, we propose a simple method of balancing the cluster voltage with only one parameter, as shown in Fig. 7.

To order for the output zero-sequence modulated voltage to be normalized, we have to normalize the multiplied currents, as shown in Fig. 7, i_{aN}, i_{bN}, and i_{cN} are the normalized values of the three-phase currents. In this paper, because

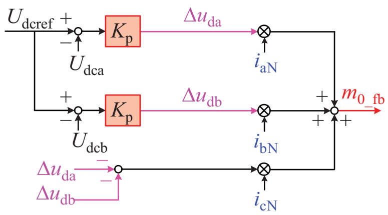

Fig. 7. Simple cluster DC voltage balancing control strategy for the CHB STATCOM without feedforward control.

negative-sequence currents are suppressed, normalized three-phase currents are expressed as:

$$\begin{bmatrix} i_{aN} \\ i_{bN} \\ i_{cN} \end{bmatrix} = \begin{bmatrix} \cos(\omega t) & -\sin(\omega t) \\ \cos\left(\omega t - \frac{2}{3}\pi\right) & -\sin\left(\omega t - \frac{2}{3}\pi\right) \\ \cos\left(\omega t + \frac{2}{3}\pi\right) & -\sin\left(\omega t + \frac{2}{3}\pi\right) \end{bmatrix} \cdot \begin{bmatrix} \frac{I_{dp}}{I_N} \\ \frac{I_{qp}}{I_N} \end{bmatrix} \quad (12)$$

Here, I_N is the rated current and has a positive value. Compared with I_{qp}, I_{dp} is nearly zero and can be ignored. We then derive the expression for the zero-sequence voltage (m_{0_fb}) with reference to Fig. 7 as:

$$\begin{aligned} m_{0\_fb} = {} & \Delta u_{da} \cdot \left(-\frac{I_{qp}}{I_N}\right) \cdot \sin(\omega t) \\ & + \Delta u_{db} \cdot \left(-\frac{I_{qp}}{I_N}\right) \cdot \sin\left(\omega t - \frac{2}{3}\pi\right) \\ & + (-\Delta u_{da} - \Delta u_{db}) \cdot \left(-\frac{I_{qp}}{I_N}\right) \cdot \sin\left(\omega t + \frac{2}{3}\pi\right) \end{aligned} \quad (13)$$

On the basis of Fig. 7 and the transformation matrix in (3), the zero-sequence voltage (m_{0_fb}) can be transformed into the dq frame, which leads to

$$\begin{aligned} M_{d0\_fb} &= \underbrace{-\frac{\sqrt{3}}{2} K_p \cdot \frac{I_{qp}}{I_N}}_{k_{p1}} \cdot (U_{dca} - U_{dcref}) \\ & \quad \underbrace{-\sqrt{3} K_p \cdot \frac{I_{qp}}{I_N}}_{k_{p2}} \cdot (U_{dcb} - U_{dcref}) \\ M_{q0\_fb} &= \underbrace{-\frac{3}{2} K_p \cdot \frac{I_{qp}}{I_N}}_{k_{p3}} \cdot (U_{dca} - U_{dcref}) \end{aligned} \quad (14)$$

Equation (14) has the same structure as (7); it is obvious that there is only one parameter K_p in (14), whereas there are four parameters in (7). To specify the range of K_p and thus satisfy inequalities (10) and (11), we substitute (14) into (6), and the cluster active power generated by the zero-sequence voltage is derived as:

$$\begin{aligned} P_{a0} &= \underbrace{\frac{-3K_p \cdot \frac{I_{qp}^2}{I_N}}{4}}_{\mathrm{KAA}} \cdot (U_{dca} - U_{dcref}) \\ P_{b0} &= \underbrace{\frac{-3K_p \cdot \frac{I_{qp}^2}{I_N}}{4}}_{\mathrm{KBB}} \cdot (U_{dcb} - U_{dcref}) \end{aligned} \quad (15)$$

In (15), the relationship between the active powers and cluster DC voltage errors is the multiplication of a coefficient (K_{AA} or K_{BB}), which indicates the active power of phase A generated by the proposed feedback control is irrelevant to the cluster DC voltage error of phase B and is related solely to the cluster DC voltage error of phase A. Similarly, the active power of phase B is irrelevant to the cluster DC voltage error of phase A and is related solely to the cluster DC voltage error of phase B, which realizes the decoupling of cluster DC voltage control between phase A and phase B. Therefore, we only force P_{a0}, and P_{b0} to be inversely proportional to the cluster DC voltage error, which means that both K_{AA} and K_{BB} are less than 0, and thus the cluster DC voltages can be balanced.

To verify this conclusion, we take phase A as an example for analysis. If the value of U_{dca} is higher than the reference value, then the value of the cluster DC voltage error of phase A ($U_{dca} - U_{dcref}$) is positive, and multiplication of this value by a negative coefficient K_{AA} produces a negative P_{a0}, which then reduces the value of U_{dca}. Similarly, phase B is also consistent with this analysis, as shown in Fig. 8. In the expressions for K_{AA} and K_{BB}, regardless of whether I_{qp} is positive or negative, terms I_{qp}^2 and I_N are constantly higher than 0, thus as long as we continue to force the parameter K_p to be positive, active power P_{a0} (P_{b0}) will remain inversely proportional to the cluster DC voltage error ΔU_{dca} (ΔU_{dcb}). In other words, the direct gain coefficients are both negative and the coupled gain coefficients are equal to zero. Hence, we can not only balance the three cluster voltages but also reduce control coupling between phases A and B. We can use the PI regulator in practical applications to eliminate cluster voltage errors in the steady state.

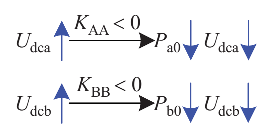

Fig. 8. Regulating mechanism of the cluster voltages.

E. Cluster DC Voltage Balancing Feedforward Control Strategy Under an Unbalanced Grid Voltage

As stated in Section II-B, unbalanced grid voltages induce uneven active powers (P_{an}, P_{bn}, and P_{cn}) among the three clusters to cause an imbalance in the three cluster voltages. The proposed control in Fig. 7 can balance the three cluster voltages using a PI regulator to generate a suitable zero-sequence voltage. However, response time of the I-regulator in PI regulators degrades dynamic performance in the transient process. To improve dynamic response, we introduce a feedforward control strategy that directly calculates the required zero-sequence voltage, which generates the regulated active power to offset the uneven active power caused by the unbalanced grid voltage. Therefore, the zero-sequence voltages generated by the feedforward control should satisfy

$$\begin{bmatrix} P_{an} + P_{a0\_ff} \\ P_{bn} + P_{b0\_ff} \\ P_{cn} + P_{c0\_ff} \end{bmatrix} = \begin{bmatrix} 0 & -\frac{I_{qp}}{2} \\ \frac{-\sqrt{3}I_{qp}}{4} & \frac{I_{qp}}{4} \\ \frac{\sqrt{3}I_{qp}}{4} & \frac{I_{qp}}{4} \end{bmatrix} \cdot \begin{bmatrix} E_{dn} \\ E_{qn} \end{bmatrix}$$

$$+\begin{bmatrix} 0 & \frac{I_{\mathrm{qp}}}{2} \\ \frac{\sqrt{3}I_{\mathrm{qp}}}{4} & \frac{-I_{\mathrm{qp}}}{4} \\ \frac{-\sqrt{3}I_{\mathrm{qp}}}{4} & \frac{-I_{\mathrm{qp}}}{4} \end{bmatrix} \cdot \begin{bmatrix} U_{\mathrm{d0\_ff}} \\ U_{\mathrm{q0\_ff}} \end{bmatrix} = \begin{bmatrix} 0 \\ 0 \\ 0 \end{bmatrix} \tag{16}$$

Here, $U_{\mathrm{d0\_ff}}$ and $U_{\mathrm{q0\_ff}}$ are the zero-sequence voltages generated by the feedforward control in the dq frame, and $P_{\mathrm{a0\_ff}}$, $P_{\mathrm{b0\_ff}}$, and $P_{\mathrm{c0\_ff}}$ are the active powers produced by $U_{\mathrm{d0\_ff}}$ and $U_{\mathrm{q0\_ff}}$ from the feedforward control. According to (16), $U_{\mathrm{d0\_ff}}$ and $U_{\mathrm{q0\_ff}}$ can be calculated as:

$$U_{\mathrm{d0\_ff}} = E_{\mathrm{dn}} \quad U_{\mathrm{q0\_ff}} = E_{\mathrm{qn}} \tag{17}$$

It is necessary to convert (17) to the abc frame to superimpose the zero-sequence modulation voltages of (17) on the output three-phase modulation voltage. Therefore, we substitute (17) into (3) and use the average of the three-phase cluster DC voltages (U_{dcref}) to standardize u_0, as follows:

$$m_{0\_\mathrm{ff}} = \frac{E_{\mathrm{dn}}\cos(\omega t) - E_{\mathrm{qn}}\sin(\omega t)}{U_{\mathrm{dcref}}} \tag{18}$$

Here, m_{0_ff} is the zero-sequence voltage from the feedforward control in the abc frame and $U_{\mathrm{dcref}} = (U_{\mathrm{dca}} + U_{\mathrm{dcb}} + U_{\mathrm{dcc}})/3$, which was already controlled in the first layer. Hence, the final zero-sequence voltage is equal to the sum of the variables from the feedback and feedforward controls. We then propose a simple cluster voltage balancing control with feedforward control, as shown in Fig. 9.

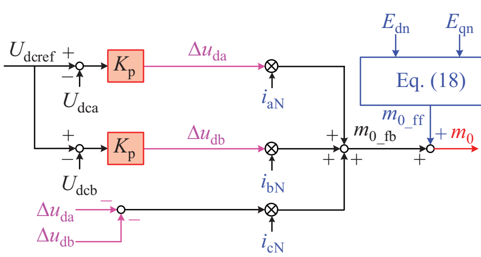

Fig. 9. Simplified cluster DC voltage balancing control strategy for the CHB STATCOM with feedforward control.

F. Comparison of Calculation Burdens between the Proposed Control and the Traditional Controls

To explain quantitatively why the proposed control is simpler than traditional controls, we present a detailed comparison on the calculation burden between traditional methods and the proposed method. Table I presents a thorough comparison of calculation burdens of the proposed control and traditional controls to quantify the simplicity of the proposed method over traditional methods. As listed in Table I, traditional controls in ([17], [19], [21]) include additional complex operations, such as square-root, cosine, and inverse trigonometric operations, which can place a greater resource burden on a controller based on a DSP or FPGA than ordinary operations (addition, subtraction, and multiplication). Although traditional control in [22] eliminates the extra complex operations, it still involves division and many ordinary operations. The proposed control not only eliminates additional complex operations but also reduces the counts of ordinary operations. In particular, the approximated consumed time of each operation item on the float-type DSP (TMS320F28335) is tested as shown in Table II.

TABLE II
CONSUMED TIME OF EACH OPERATION ITEM ON THE TMS320F28335

Operation item	Approximated consumed time (µs)
Addition or Subtraction	0.06
Multiplication	0.06
Division	1.7
Square Root	1.2
Cosine	1.1
Inverse Tangent	4.7

To further highlight the advantages of the proposed control, we take the core dual-loop control as a comparison. The approximate consumed time of the core dual-loop control is 0.96 µs. From Table II, time consumed for an inverse tangent, cosine, or square root operation is much greater than consumed for addition, subtraction, or multiplication. Additionally, the approximate time consumed for traditional control in [17] is 41.67 µs, which is roughly 43 times longer than of the core double-loop control, and the corresponding time in [19] is 16.36 µs, which is roughly 17 times longer than of the core double-loop control, while the corresponding time in [21] is 19.72 µs which is about 20 times longer than of the core double-loop control, and the

corresponding time in [22] is 6.88 µs which is approximately 7 times longer than of the core double-loop control, but the approximate time consumed by the proposed control method is only 0.84 µs, which is 0.875 times that of the core double-loop control.

As a result, the proposed control not only requires no complex operations and fewer ordinary operations in deriving the zero-sequence voltage, which is simpler than traditional controls but also can greatly simplify the software algorithm of the overall system control.

TABLE I
COMPARISON ON THE CALCULATION BURDENS BETWEEN THE PROPOSED AND TRADITIONAL CONTROLS

Operation item	The proposed control (Operation counts)	The traditional control in [17] (Operation counts)	The traditional control in [19] (Operation counts)	The traditional control in [21] (Operation counts)	The traditional control in [22] (Operation counts)
Addition or Subtraction	7	22	19	36	28
Multiplication	7	12	5	36	30
Division	0	5	2	3	2
Square Root	0	0	1	1	0
Cosine	0	15	1	1	0
Inverse Tangent	0	2	2	1	0
Comparison	0	1	0	2	0

III. Simulation Results

Simulations were executed with MATLAB/Simulink and the proposed control strategy was validated for the two cases. The simulation parameters are given in Table III.

TABLE III
SIMULATION PARAMETERS

Quantity	Sign	Value
Rated reactive power capacity	Q	7.5 kvar
RMS value of grid line voltage	U_s	400 V
Cascaded cell number	N	5
AC filter inductance	L	9 mH
Rated DC voltage	U_{dc}	85 V
DC capacitance	C	3 mF

A. Performance of the Proposed Cluster DC Voltage Balancing Control in the Balanced Scenario

DC-side loss inconsistency is one of the reasons for the imbalance among the three clusters. In this case, to validate the performance of the proposed control, we connected the DC links of the CHB converter in parallel with different power resistors, where each cell of phases A and C have a 300-Ω resistor connected in parallel on the DC-side and no cell of phase B has a parallel resistor. Figs. 10(a) and 10(b) present the grid voltages and currents under normal conditions respectively; it is seen that both parameters are balanced. As illustrated in Fig. 10(c), the proposed control is inactive until moment t_0, when DC voltages of the three clusters are imbalanced. When the proposed control is activated, the normalized zero-sequence modulated voltage (m_0) is generated to eliminate deviation among the three cluster voltages from the reference value of 425 V to achieve cluster DC voltage balance, as shown in Fig. 10(c) and 10(d).

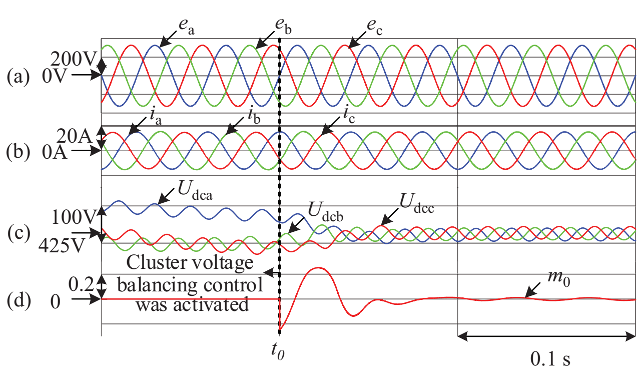

Fig. 10. Simulation waveforms obtained with the proposed cluster voltage balancing control under different power resistors.

B. Performance of the Proposed Cluster DC Voltage Balancing Control Under the Unbalanced Grid Voltages

Under the unbalanced grid voltages, a comparison was made for the following two cases. All the simulation parameters were set equal to those in Section III.A. The only difference between the cases was the introduction of feedforward control in case 1 and removal of feedforward control in case 2.

Case 1: The feedforward control modeled in Section II-E is added to the proposed control. As illustrated in Fig. 11(a),

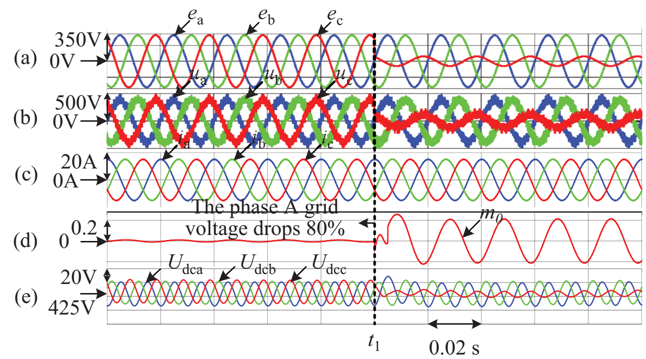

Fig. 11. Simulation waveforms obtained with the proposed cluster DC voltage balancing control under the unbalanced grid voltages.

at moment t_1, the phase-C grid voltage decreases by 80%. To balance the phase currents, the output staircase voltages of STATCOM also become unbalanced, as depicted in Fig. 11(b). Waveforms of the rated positive-sequence capacitive reactive power currents compensated by the STATCOM are presented in Fig. 11(c). It is evident that balance can be maintained even during voltage drop of the phase-C grid. As indicated in Fig. 11(d), after moment t_1, a normalized zero-sequence modulated voltage is generated by the proposed control to reallocate the three cluster active powers. In summary, the proposed control is capable of balancing the three cluster DC voltages at the reference value of 425 V in the transient process even for the unbalanced grid voltages, as seen in Fig. 11(e).

Case 2: In this case, the feedforward control is withdrawn and only feedback control is retained. Cluster DC voltage is balanced entirely by the zero-sequence voltage generated by feedback control. Fig. 12 shows when phase-C grid voltage drops by 80% at t_1, the three cluster DC voltages converge so slowly that they still have not completely converged to their reference value (425 V) 0.3 s after moment t_1, and their dynamic performance is much worse than in the case of Fig. 11(e). Therefore, the three cluster DC voltages have slow dynamic response in unbalanced grid voltages without feedforward control.

IV. Experimental Results

Theoretical analysis described in the former sections is verified using an experimental prototype of the star-connected CHB STATCOM. The main circuit parameters of the experimental platform are the same as in Table III, and a photograph of the experimental platform is shown in Fig. 13.

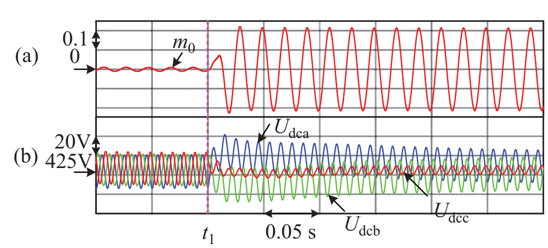

Fig. 12. Simulation waveforms obtained under the unbalanced power grid without feedforward control.

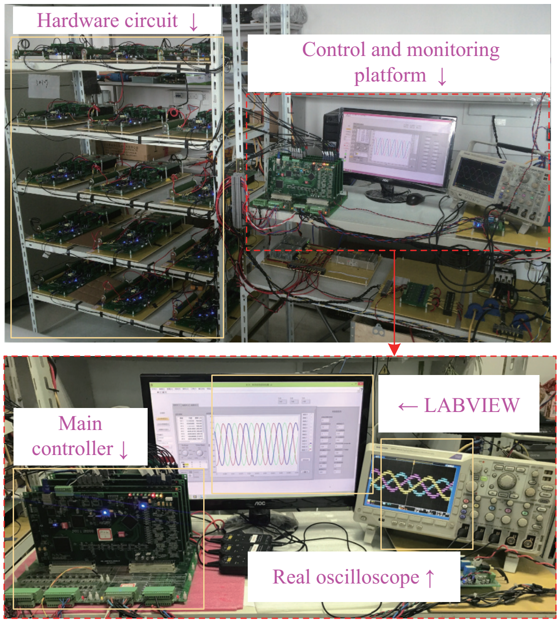

Fig. 13. Experimental setup.

DSP- and FPGA-based controllers are used to sample currents and voltages, and all sampled signals are transmitted to a computer through the Ethernet. In addition, we developed a virtual oscilloscope in LabVIEW to display voltage and current waveforms.

A. Normal Operation Under a Balanced Power Grid

To experimentally verify the proposed strategy, we simulated DC-side losses equivalent to those in the setup described in Section III.A. STATCOM only compensates for rated capacitive reactive power currents as shown in Fig. 14(a). The zero-sequence voltage is not injected before moment t_0, and the three cluster voltages are therefore, not balanced. When the proposed control is activated, normalized zero-sequence modulated voltage is generated to balance the three cluster DC voltages, where the three cluster DC voltages are balanced to the reference value of 425 V after a short dynamic process, as shown in Figs. 14(b) and 14(c).

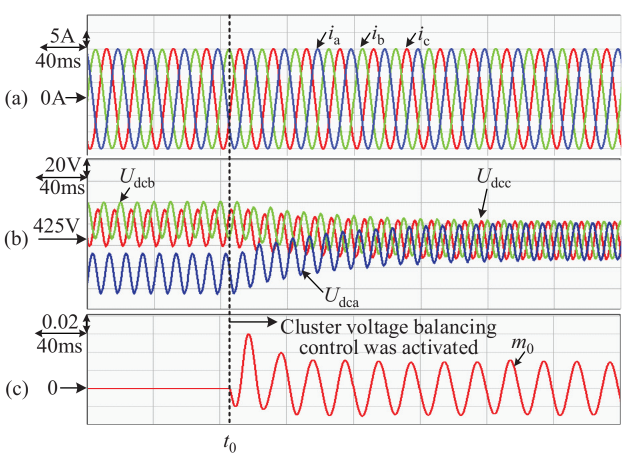

Fig. 14. Experimental results obtained with the proposed control of inconsistent DC-side losses under the balanced condition.

B. Results of Cluster Voltage Balancing Control with the Proposed Control under an Unbalanced Grid Voltage

We set an imbalanced situation on the grid as phase-A grid voltage falls by 80% at moment t_0, as shown in Fig. 15(a). To suppress negative-sequence current to achieve he three-phase current balance, the output voltages of STATCOM become unbalanced after t_0, as seen in Fig. 15(b). Fig. 15(c) presents the waveform of the output rated capacitive reactive current, which can be seen to maintain normal current output despite the unbalanced drop in grid-side voltage at moment t_0. After the proposed control is activated, a zero-sequence modulated voltage is generated to redistribute the active powers of the three clusters, so the three cluster voltages remain balanced at 425 V under unbalanced grid voltage even during the transient process, as shown in Fig. 15(d) and 15(e).

For verification of the effectiveness of the feedforward control, we set the same operating conditions as in Fig. 15 except the feedforward control is removed. In this scenario, the zero-sequence voltage is generated by the feedback control to balance the three cluster voltages. Fig. 16(b) shows when phase A grid voltage dips at moment t_0, it takes approximately

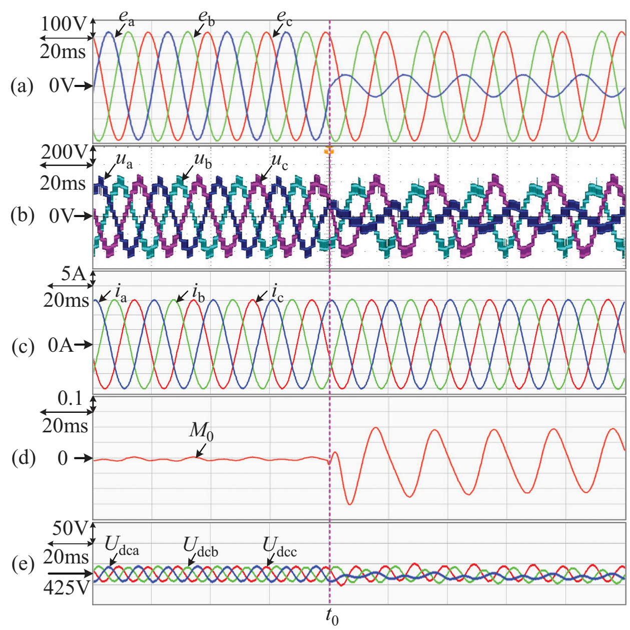

Fig. 15. The experimental waveforms with the proposed control scheme under unbalanced grid voltage.

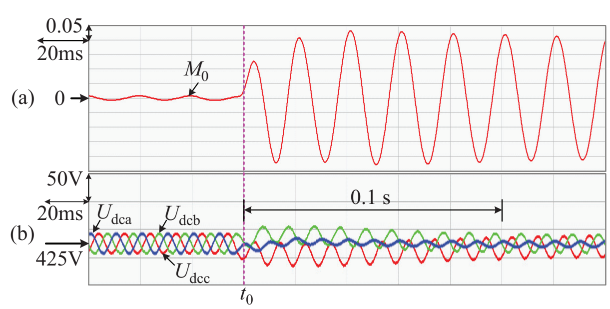

Fig. 16. Experimental results obtained in the unbalanced scenario without the feedforward control.

0.1 s for the three cluster DC voltages to balance to the reference value of 425 V. Compared with experimental results in Fig. 15(e), dynamic response of the proposed control without the feedforward control is poor. The proposed feedforward control thus improves dynamic performance of the cluster DC voltage balancing in the unbalanced scenario.

V. Conclusion

We have represented the zero-sequence voltages in the dq frame instead of considering the relationship between the amplitude and phase angle. The DC component is linearly regulated by the PI regulator, which eliminates many complex calculations such as those of division, trigonometric operations, inverse trigonometric operations, and square root operations. Therefore, the proposed cluster DC voltage balancing control is computationally simpler and consumes fewer controller resources than traditional zero-sequence voltage injection controls. Analysis of the theory is verified in simulations and experiments, with results demonstrating the proposed cluster DC voltage control performs well in both balanced and unbalanced cases.

References

[1] H. Liu, L. Ma, W. Song, L. Peng, S. Cheng and Y. Liao, "A voltage balancing method based on H∞ optimal control for single-phase cascaded H-bridge rectifiers," in *CSEE Journal of Power and Energy Systems*, doi: 10.17775/CSEEJPES.2022.04770.

[2] T. Zhao and D. L. Chen, "A power adaptive control strategy for further extending the operation range of single-phase cascaded H-bridge multilevel PV inverter," *IEEE Transactions on Industrial Electronics*, vol. 69, no. 2, pp. 1509–1520, Feb. 2022, doi: 10.1109/TIE.2021.3060646.

[3] T. Zhao and D. L. Chen, "Analysis and suppression of active power backflow of three-phase common DC-bus cascaded H-bridge PV grid-connected inverter during LVRT," *IEEE Journal of Emerging and Selected Topics in Power Electronics*, vol. 10, no. 1, pp. 745–759, Feb. 2022, doi: 10.1109/JESTPE.2021.3071091.

[4] P. R. Kasari and S. Bhattacharjee, "An HESS Based on a Modified MMCC-TSBC Converter Integrating Energy Storages," in *CSEE Journal of Power and Energy Systems*, vol. 9, no. 5, pp. 1698–1709, Sept. 2023, doi: 10.17775/CSEEJPES.2022.02800.

[5] S. Kundu, S. Bhowmick, and S. Banerjee, "Improvement of power utilisation capability for a three-phase seven-level CHB inverter using an improved selective harmonic elimination–PWM scheme by sharing a desired proportion of power among the H-bridge cells," *IET Power Electronics*, vol. 12, no. 12, pp. 3242–3253, Oct. 2019.

[6] H. Akagi, "Classification, terminology, and application of the Modular Multilevel Cascade Converter (MMCC)," *IEEE Transactions on Power Electronics*, vol. 26, no. 11, pp. 3119–3130, Nov. 2011.

[7] E. Behrouzian and M. Bongiorno, "Investigation of negative-sequence injection capability of cascaded H-bridge converters in star and delta configuration," *IEEE Transactions on Power Electronics*, vol. 32, no. 2, pp. 1675–1683, Feb. 2017.

[8] A. M. Vural, "Self-capacitor voltage balancing method for optimally hybrid modulated cascaded H-bridge D-STATCOM," *IET Power Electronics*, vol. 9, no. 14, pp. 2731–2740, Nov. 2016.

[9] F. Z. Peng, J. S. Lai, J. W. McKeever, and J. VanCoevering, "A multilevel voltage-source inverter with separate DC sources for static VAr generation," *IEEE Transactions on Industry Applications*, vol. 32, no. 5, pp. 1130–1138, Sep./Oct. 1996.

[10] H. Akagi, S. Inoue, and T. Yoshii, "Control and performance of a transformerless cascade PWM STATCOM with star configuration," *IEEE Transactions on Industry Applications*, vol. 43, no. 4, pp. 1041–1049, Jul./Aug. 2007.

[11] N. Hatano and T. Ise, "A configuration and control method of cascade H-bridge STATCOM," in *IEEE Power and Energy Society General Meeting - Conversion and Delivery of Electrical Energy in the 21st Century*, Pittsburgh, PA, 2008, pp. 1–8.

[12] N. Hatano, and T. Ise, "Control scheme of cascaded H-bridge STATCOM using zero-sequence voltage and negative-sequence current," *IEEE Transactions on Power Delivery*, vol. 25, no. 2, pp. 543–550, Apr. 2010.

[13] C. T. Lee, B. S. Wang, S. W. Chen, S. F. Chou, J. L. Huang, P. T. Cheng, H. Akagi, and P. Barbosa, "Average power balancing control of a STATCOM based on the cascaded H-bridge PWM converter with star configuration," *IEEE Transactions on Industry Applications*, vol. 50, no. 6, pp. 3893–3901, Nov./Dec. 2014.

[14] Y. J. Shi, B. Y. Liu, Y. J. Shi, and S. X. Duan, "Individual phase current control based on optimal zero-sequence current separation for a star-connected cascade STATCOM under unbalanced conditions," *IEEE Transactions on Power Electronics*, vol. 31, no. 3, pp. 2099–2110, Mar. 2016.

[15] D. R. Lu, S. Wang, J. H. Yao, T. Y. Yang, and H. B. Hu, "Cluster voltage regulation strategy to eliminate negative-sequence currents under unbalanced grid for star-connected cascaded H-bridge STATCOM," *IEEE Transactions on Power Electronics*, vol. 34, no. 3, pp. 2193–2205, Mar. 2019.

[16] S. X. Du and J. J. Liu, "A brief comparison of series-connected modular topology in STATCOM application," in *Proceedings of ECCE Asia Downunder (ECCE Asia)*, 2013, pp. 456–460.

[17] Q. Song, and W. H. Liu, "Control of a cascade STATCOM with star configuration under unbalanced conditions," *IEEE Transactions on Power Electronics*, vol. 24, no. 1, pp. 45–58, Jan. 2009.

[18] L. Maharjan, S. Inoue, H. Akagi, and J. Asakura, "State-of-charge (SOC)-balancing control of a battery energy storage system based on a cascade PWM converter," *IEEE Transactions on Power Electronics*, vol. 24, no. 6, pp. 1628–1636, Jun. 2009.

[19] K. Sano and M. Takasaki, "A transformerless D-STATCOM based on a multivoltage cascade converter requiring No DC sources," *IEEE Transactions on Power Electronics*, vol. 27, no. 6, pp. 2783–2795, Jun. 2012.

[20] J. I. Y. Ota, Y. Shibano, N. Niimura, and H. Akagi, "A phase-shifted-PWM D-STATCOM using a modular multilevel cascade converter (SSBC)—part I: modeling, analysis, and design of current control," *IEEE Transactions on Industry Applications*, vol. 51, no. 1, pp. 279–288, Jan./Feb. 2015.

[21] H. C. Chen, P. H. Wu, C. T. Lee, C. W. Wang, C. H. Yang, and P. T. Cheng, "Zero-sequence voltage injection for DC capacitor voltage balancing control of the star-connected cascaded H-bridge PWM converter under unbalanced grid," *IEEE Transactions on Industry Applications*, vol. 51, no. 6, pp. 4584–4594, Nov./-Dec. 2015.

[22] D. R. Lu, J. X. Zhu, J. F. Wang, J. H. Yao, S. Wang, and H. B. Hu, "A simple zero-sequence-voltage-based cluster voltage balancing control and the negative sequence current compensation region identification for star-connected cascaded H-bridge STATCOM," *IEEE Transactions on Power Electronics*, vol. 33, no. 10, pp. 8376–8387, Oct. 2018.

[23] Z. Liu, B. Y. Liu, S. X. Duan, and Y. Kang, "A novel DC capacitor voltage balance control method for cascade multilevel STATCOM," *IEEE Transactions on Power Electronics*, vol. 27, no. 1, pp. 14–27, Jan. 2012.

Kai Hu received the B.S. degree in the School of Electrical and Automation Engineering from Hefei University of Technology, Hefei, China, in 2019. He is currently working toward the Ph.D. degree in the School of Electrical and Automation Engineering, Hefei University of Technology, Hefei, China. His research interests include the control of multilevel converters.

Guoliang Zhao received B.S., M.S. and Ph.D. degrees in Electrical Engineering from North China Electric Power University, Beijing, China, in 2015. He is currently with the State Key Laboratory of Advanced Power Transmission Technology (State Grid Smart Grid Research Institute), Beijing, China. His research interests include power electronics and high voltage technology.

Daorong Lu received the B.S. degree in Electrical Engineering from Nanjing Normal University, Nanjing, China, in 2013, and the Ph.D. degree in Electrical Engineering from Nanjing University of Aeronautics and Astronautics, Nanjing, China, in 2018. He is currently a Lecturer with the School of Electrical and Automation Engineering, Nanjing Normal University, Nanjing, China. In 2019, he was with the College of Automation Engineering, Nanjing University of Aeronautics and Astronautics, Nanjing, China, as a Postdoctoral Research Fellow. His research interests include topology and control of multilevel converters and power quality devices.

Zhengang Lu received the B.S. degree in Electrical Engineering and Automation from Xi'an Jiaotong University in 2007, and the M.S. degree in Power Electronics from the China Electric Power Research Institute (CEPRI) in 2010. He is currently working in Stated Grid Smart Grid Research Institute (SGRI), Beijing, China. He is also working toward the Ph.D. degree in Xi'an Jiaotong University. From 2010 to 2012, he was an Assistant R&D Engineer with the Power Electronics Department in CEPRI. Since 2012, he has been a Senior R&D Engineer with the Power Electronics Department, SGRI. His research interests include FACTS and novel power transmission technology.

Nianwen Xiang received B.S. and M.S. degrees in Electrical and Electronics Engineering from Wuhan University, Wuhan, China, in 2007 and 2009, respectively, and the Ph.D. degree in Electrical Engineering from North China Electric Power University, Beijing, China, in 2017. He is currently a Professor at the School of Electrical Engineering and Automation, Hefei University of Technology, Hefei, China. His research interests include electromagnetic compatibility and lightning protection technology for power systems and railway systems, electrical insulation and materials, and condition monitoring of power apparatus.

Shulai Wang received the B.S degree in Electrical Engineering and Automation in 2019 from Anhui Jianzhu University, Anhui, China. He is currently working toward the Ph.D. degree in the School of Electrical Engineering and Automation, Hefei University of Technology. Hefei, China. His current research interests include electromagnetic transient characteristics of the flexible low-frequency transmission system.

Jintian Lin received the B.E. degree and the M.S degree in Electrical Engineering from Southwest Jiaotong University, Chengdu, China in 2016 and 2019, respectively. Now he is working in the Power grid Technology Center of State Grid Zhejiang Electric Power Research Institute, Hangzhou, China. His major scientific interest is focused on power system source-grid coordination and advanced power transmission technology.